Mechanically Robust, Flame-Retardant Poly(lactic acid) Biocomposites via Combining Cellulose Nanofibers and Ammonium Polyphosphate

Weida Yin,[†] Lei Chen,[‡] Fengzhu Lu,[‡] Pingan Song,*[,‡,§] Jinfeng Dai,*[,‡] and Linghui Meng*[,†]

[†]School of Chemical Engineering and Technology, Harbin Institute of Technology, 92 West Dazhi Street, Nangang District, Harbin 150001, China

[‡]Department of Materials, College of Engineering, Zhejiang A & F University, 666 Wusu Street, Linan District, Hangzhou 311300, China

[§]Center for Future Materials, University of Southern Queensland, West Street, Toowoomba, Queensland 4350, Australia

ABSTRACT: Expanding the application range of flame-retardant polymer biocomposites remains a huge challenge for a sustainable society. Despite largely enhanced flame retardancy, until now the resultant poly(lactic acid) (PLA) composites still suffer reduced tensile strength and impact toughness due to improper material design strategies. We, herein, demonstrate the design of a green flame retardant additive (ammonium polyphosphate (APP)@ cellulose nanofiber (CNF)) via using the cellulose nanofibers (CNFs) as the green multifunctional additives hybridized with ammonium polyphosphate (APP). The results show that PLA composite with 5 wt % loading of APP@CNF can pass the UL-94 V-0 rating, besides a high limited oxygen index of 27.5%, indicative of a significantly enhanced flame retardancy. Moreover, the 5 wt % of APP@CNF enables the impact strength (σ_i) of the PVA matrix to significantly improve from 7.63 to 11.8 kJ/m^2 (increase by 54%), in addition to a high tensile strength of 50.3 MPa for the resultant flame-retardant PLA composite. The enhanced flame retardancy and mechanical strength performances are attributed to the improved dispersion of APP@CNF and its smaller phase size within the PLA matrix along with their synergistic effect between APP and CNF. This work opens up a facile innovative methodology for the design of high-performance ecofriendly flame retardants and their advanced polymeric composites.
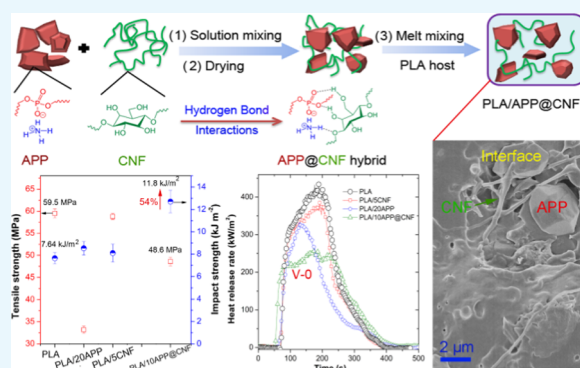
1. INTRODUCTION

Nowadays, petrochemical polymeric materials are under tremendous impact due to the depletion of fossil resources and the sustainable development of our society.[1,2] Currently, poly(lactic acid) (PLA) is considered as one of the most promising renewable biomass material with excellent mechanical properties, biodegradability, transparency, and so on.[3−5] These attractive properties allow PLA to find growing application potentials in packaging, electric and electronic, automotive, textiles, and transportation. However, the intrinsic flammability of PLA, which has a low limited oxygen index (LOI) of only 19%, extremely restricts its applications in the above fields. Therefore, it is highly urgent to endow PLA with desired flame retardancy to meet the fire-retardant requirement. Especially a UL-94 V-0 level during fire is required in electric industrial applications.[6−9]

Tremendous efforts have been made to improve the flame retardancy of PLA to date. Among the current flame retardancy approaches, inorganic phosphorus-containing intumescent flame retardants have been identified as a promising approach because of relatively high efficiency, low smoke, and low toxicity.[10−13] However, currently the flame-retardant PLA composites normally show reduced mechanical properties relative to the PLA bulk. For example, Song et al. incorporated a combination of ammonium polyphosphate (APP)/poly-(ethylene glycol) 6000 into PLA, and the addition of 7 wt % of this combined system can make PLA pass a V-0 rating. Unfortunately, the tensile strength significantly decreases in spite of largely increased strain at break.[8] Recently, Zhao et al. have synthesized one superefficient flame retardant N,N'-diallyl-P-phenylphosphonicdiamide (P-AA), and only adding 1.0 wt % P-AA enables PLA to pass the UL-94 V-0 rating without compromising the tensile strength of PLA.[14] However, the ductility of PLA is reduced to a certain degree probably due to the cross-link action between P-AA and PLA.[14] Therefore, a lot of efforts are focused on designing a new type of flame retardant or introducing a reinforcement component for improving the mechanical properties of the flame-retardant
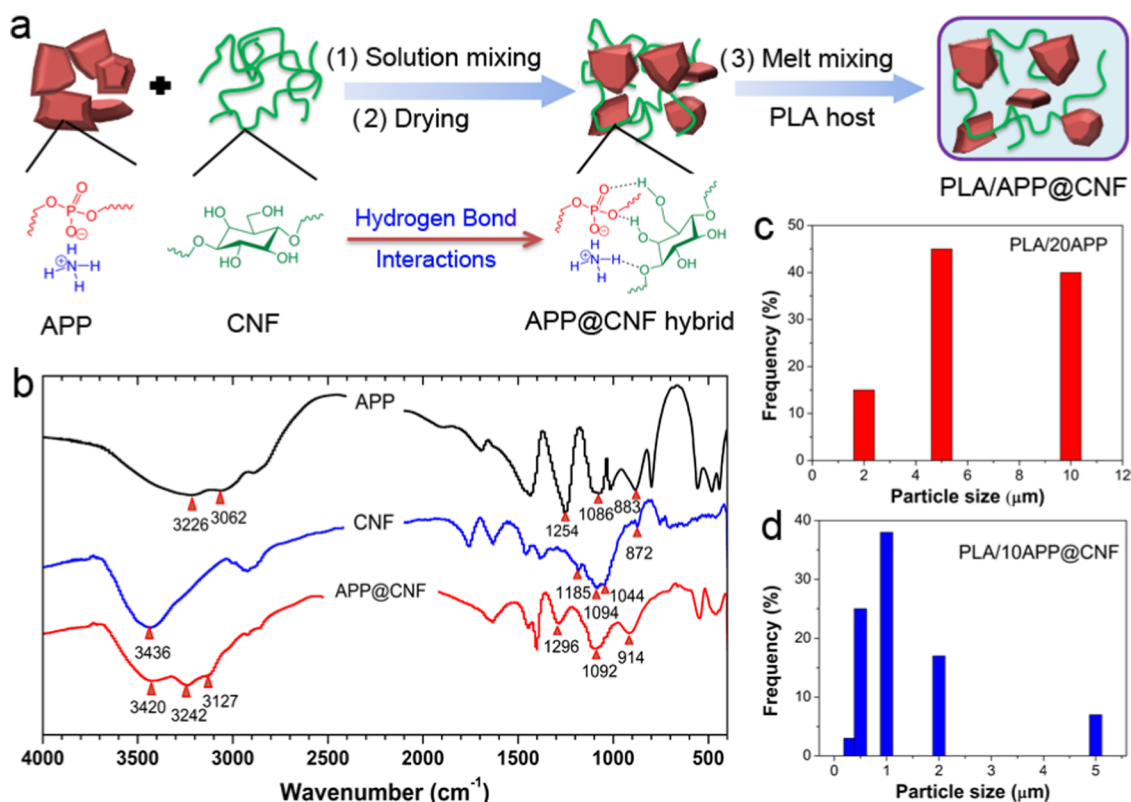
Figure 1. (a) Illustration of the schematic representation of the design and fabrication process for both APP@CNF and its PLA composite. (b) IR spectra of APP, CNF, and APP@CNF, and the weight-average particle size (d_w) distribution of (c) 20% APP and (d) 10% APP@CNF within the PLA matrix.

PLA composites.[15−17] A typical example is that the direct use of nanofibrous cellulose (NFC) or modified NFC in the APP-flame-retarded PLA composites significantly decreases the mechanical strength of the PLA composites due to the negative dispersion in PLA and poor interfacial adhesion.[15]

Meanwhile, the effect of rodlike aluminated mesoporous silica (Al-SBA) on the flame retardancy of PLA was investigated by Qian et al.[16] The results show that PLA composite with 0.5 wt % Al-SBA can get a V-0 rating during UL-94 tests and basically maintain the tensile strength of the PLA. We have recently designed a novel core−shell flame-retardant system by chemically grafting the phosphorus−nitrogen-based polymer on the surface of cellulose nanofiber (CNF). Specifically, adding 10 wt % of this flame retardant enables PLA composite to achieve a UL-94 V-0 rating and show a significantly reduced peak heat release rate (pHRR), indicating a good flame retardancy. Unexpectedly, the tensile strength of the PLA composite increases by about 24% as compared with that of the PLA matrix.[17] Despite that, currently the preparation of these synthesized flame-retardant systems is normally not cost-effective and ecofriendly, for instance, the toxic solvents or raw materials are involved in some cases. Therefore, it remains a major challenge to design high-performance flame retardants by using facile material design strategies.

Because of its exceptional mechanical strength and stiffness,[18−20] one-dimensional CNF can act as a reinforcing agent for the flame-retardant polymer composites and also for the char layer during the combustion of the material.[17] In addition, it can also serve as the surface modifier for the flame retardant, APP. Therefore, we herein have demonstrated the facile preparation of a new hybridized flame-retardant system

(APP@CNF) through facilely ball-milling mixing APP and CNF in water by using CNF as the surface modifier and the synergistic agent for APP. The results show that the presence of CNF improves the dispersion of APP within the PLA matrix, and a loading level as low as 5 wt % of APP@CNF enables PLA to pass a V-0 rating in addition to a LOI of 27.5%. Moreover, 5 wt % of APP@CNF enables the impact strength (σ_i) for the PVA matrix to improve from 7.63 to 11.8 kJ/m^2 (increase by 54%), besides a high tensile strength of 50.3 MPa for the resultant PLA composite. This work offers a facile ecofriendly methodology to create high-performance green flame-retardant additives and their advanced polymer composites.

2. RESULTS AND DISCUSSION

2.1. Characterization of APP@CNF. Fourier transform infrared (FT-IR) spectra of APP, CNF, and APP@CNF are performed to characterize their chemical structure and hydrogen-bond (H-bond) interactions. As shown in Figure 1b, the pure APP shows several characteristic absorption peaks. The absorption band at 3226 cm^{-1} is attributed to the stretching vibration of N−H groups and the peak around 1254 cm^{-1} is assigned to the P=O stretching vibration. The peaks at 1086 and 883 cm^{-1} belong to the asymmetric stretching vibration of P−O.[21] In the case of pure CNF, these are typical characteristic absorption peaks of CNF, such as 3436 cm^{-1} (ν_{O-H}), 1185 cm^{-1} (ν_{C-H}), 1094 cm^{-1} (ν_{-O-}), 1044 cm^{-1} (ν_{C-O}).[17] The spectrum of APP@CNF basically shows the characteristic absorption peaks of both APP and CNF. Moreover, compared to APP and CNF, several new absorption bands appear at 3127, 3242, and 3240 cm^{-1}, belonging to the stretching vibration of bonded N−H and O−H groups between
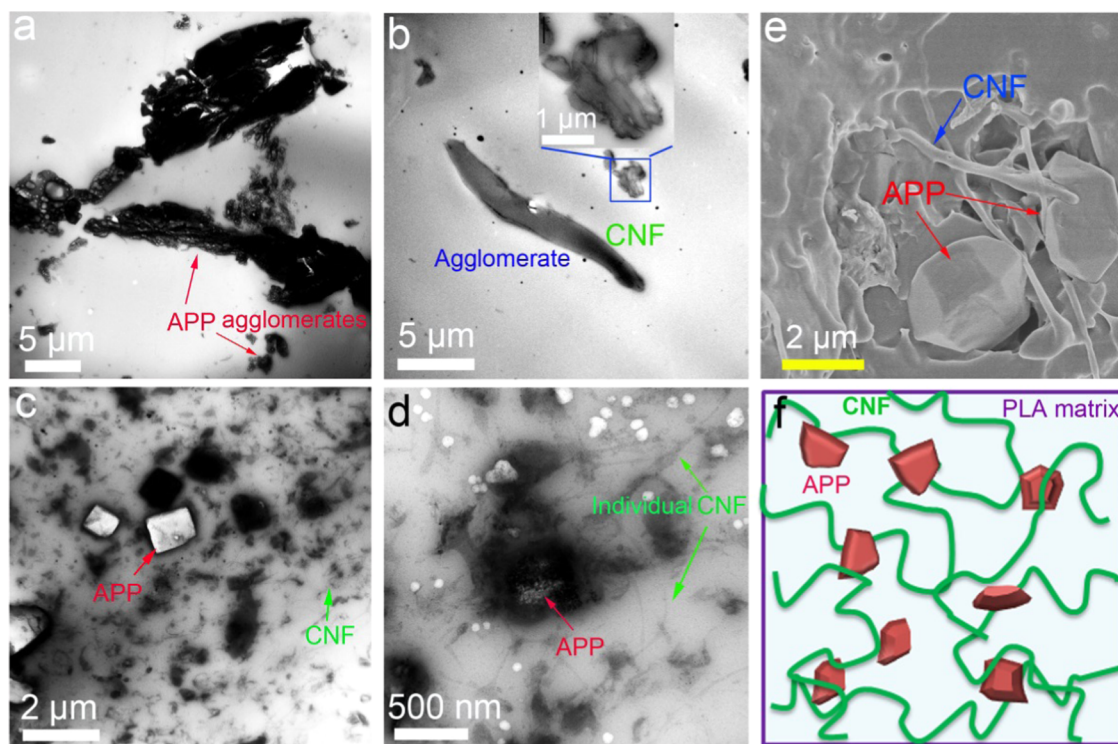
Figure 2. TEM images of (a) PLA/20APP, (b) PLA/5CNF, and (c, d) PLA/10APP@CNF. (e) SEM image of PLA/10APP@CNF. (f) Schematic illustration for the dispersion of both APP and CNF within PLA host, as well as their interactions.
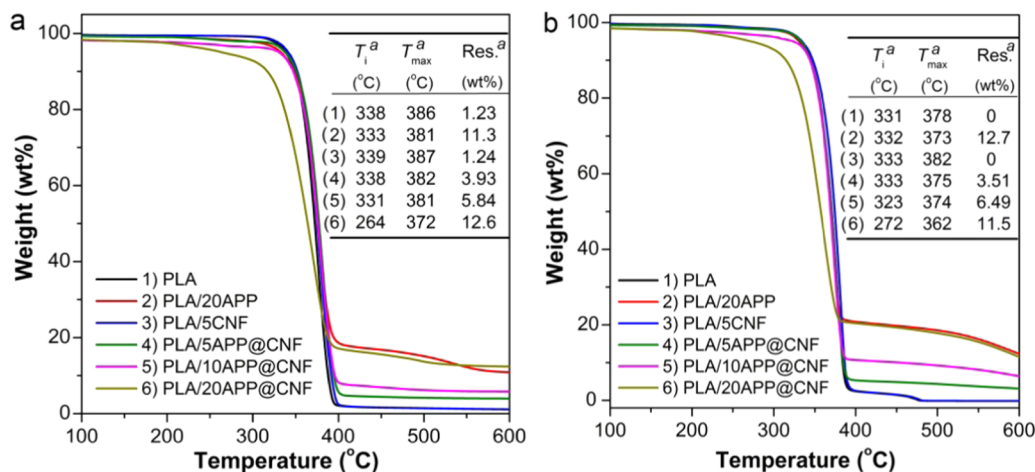
Figure 3. TGA curves of PLA and its biocomposites based on the APP, CNF, and APP@CNF in (a) nitrogen and (b) air conditions.

APP and CNF. In addition, the stretching vibration of P=O of APP shows a blueshift from 1254 to 1296 cm^{-1}, indicating strong H-bond interactions between O−H groups on the CNF surface and P=O in APP. This is reasonable that abundant hydroxyl groups on the CNF surface can strongly interact with both N−H and P=O groups in APP via the formation of H-bonds.[22,23] To examine the phase size of APP@CNF and APP within the PLA matrix, the weight-average particle size distribution of 20 wt % APP and 10 wt % APP@CNF within the PLA composite are analyzed (Figure 1c,d). Unexpectedly, APP@CNF shows a statistical weight-average diameter (d_w) of 0.5−1.0 μm except for some big phases, which is much smaller than d_w (2−10 μm) of APP in the PLA matrix. This is because the presence of CNF during the ball-milling process helps reduce the phase size of APP by acting as a surface modifier.

2.2. Dispersion of APP@CNF. The surface morphology and dispersion of APP, CNF, APP@CNF, and PLA composites are visually observed by transmission electron microscopy (TEM) and scanning electron microscopy (SEM). As displayed in Figure 2a, many APP agglomerates (marked by red arrows) appear in the PLA/20APP composite because the great polarity difference between APP and PLA makes them thermodynamically incompatible. Similarly, the CNF also exists basically in the form of agglomeration in the PLA matrix (see Figure 2b) due to the strong polarity of the CNF. In comparison, APP@ CNF can homogeneously disperse within the PLA matrix and no obvious interfaces can be recognized between APP@CNF and the polymer matrix, as presented in Figure 2c,e. At a high magnification, the individual CNF (marked by the green arrow) and nanoscale APP (marked by red arrow) can be identified.

Table 1. Detailed Flame Retardancy Data for PLA and its Flame-Retardant Composites Obtained from the Cone Calorimeter, LOI, and UL-94 Measurements

run	t_{ign}[a] (s)	pHRR[a] (kJ/m^2)	THR[a] (MJ/m^2)	AMLR[a] (g/s)	TSR[a] (m^2/m^2)	char[a] (wt %)	LOI (vol %)	UL-94 ratings	dripping Y/N
PLA	69 ± 1	434 ± 25	70.1 ± 0.5	0.079 ± 0.007	1.816	0.56	19.5	NR	Y
PLA/20APP	61 ± 1	328 ± 20	47.1 ± 0.4	0.059 ± 0.006	57.27	25.8	30.5	V-0	N
PLA/5CNF	67 ± 1	386 ± 22	62.4 ± 0.4	0.100 ± 0.01	0.6363	0.57	20.0	V-2	Y
PLA/5APP@CNF	48 ± 1	375 ± 15	56.6 ± 0.5	0.074 ± 0.008	55.03	4.93	27.5	V-0	N
PLA/10APP@CNF	51 ± 1	255 ± 15	57.9 ± 0.6	0.067 ± 0.009	106.6	7.32	30.0	V-0	N
PLA/20APP@CNF	60 ± 1	193 ± 17	53.6 ± 0.5	0.052 ± 0.004	142.7	14.4	32.5	V-0	N

[a]t_{ign}, pHRR, THR, average mass loss rate (AMLR), TSR, and char refer to the time to ignition, peak heat release rate, total heat rate, total smoke release, and char residue, respectively.
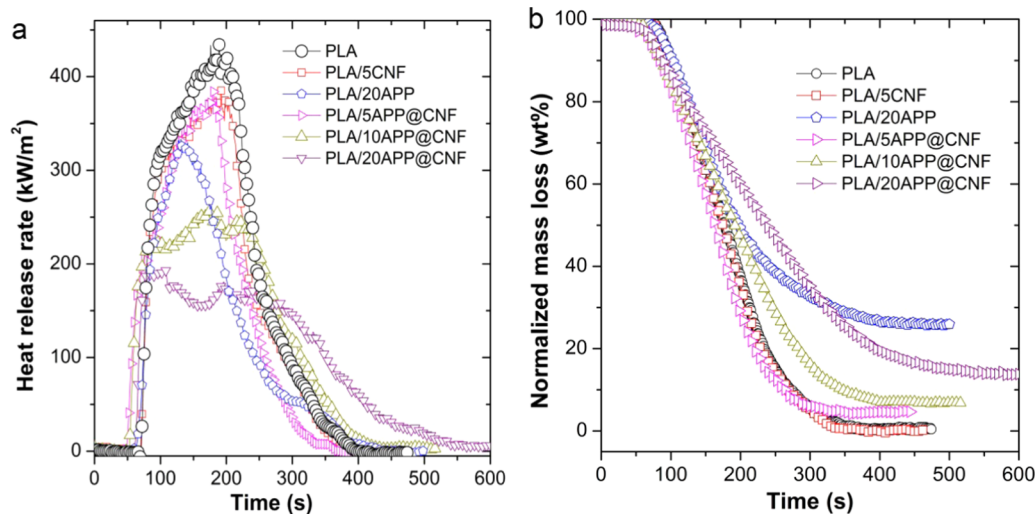
Figure 4. (a) Heat release rate and (b) normalized mass loss curves of PLA and its biocomposites based on APP, CNF, and APP@CNF at an incident heat flux of 35 kW/m^2.

Furthermore, as seen clearly in Figure 2c,d, the CNF phase locates around the APP surface by acting as surface modifier. This interesting phenomenon indicates that through hybridization, the CNF enables APP to well disperse in the PLA matrix by acting as the interfacial adhesion agent between PLA and APP. Figure 2f gives a schematic illustration of the dispersion and interactions of both CNF and APP within the PLA matrix.

2.3. Thermal Properties. Figure 3 presents the thermogravimetric analysis (TGA) curves of PLA and its composites based on APP, CNF, and APP@CNF under nitrogen and air conditions. In nitrogen, the pristine PLA shows a relatively high thermal stability with an initial degradation temperature (T_i) of 338 °C, and holds only a small amount of 1.23 wt % char residue at 600 °C. PLA/5CNF begins to degrade at 339 °C. The maximum weight loss occurs at temperature (T_{max}) 387 °C, with only 1.24 wt % char residue at 600 °C, very close to that of the PLA. In comparison, upon introducing APP into the PLA matrix, PLA/20APP exhibits a slight lower T_i of 333 °C but a much higher char residue of 11.3 wt % than PLA and PLA/5CNF, this is probably because APP can catalyze the esterification and decomposition of PLA at the beginning of the degradation stage and then promote the formation of char. For PLA/APP@CNF, the decrease in T_i becomes more pronounced with increasing APP@CNF content. Despite that, the char residue at 600 °C of APP@CNF significantly increases from 3.93 to 12.6 wt % when the addition of APP@CNF increases from 5 to 20 wt %. Interestingly, PLA/20APP@CNF

displays a much lower T_i of 264 °C, but a little higher char residue (12.6 wt %) than that of PLA/20APP. It is probably attributed to the fact that APP can also catalyze the dehydration of CNF to generate char. In addition, the trend of the TGA results of PLA and its biocomposites in air atmosphere (as shown in Figure 3b) are very similar to those in nitrogen. However, it should be noted that PLA/10APP@CNF still maintain a relatively high T_i of 323 °C, which means that the PLA/APP@CNF systems are still thermostable and can endure a relatively high melt-processing window.

2.4. Flame Retardancy. Limiting oxygen index (LOI) and vertical burning behaviors are used to evaluate the flame-resistant properties of PLA composites,[24] as summarized in Table 1. The pristine PLA only shows a LOI value of 19.5% and has no rating in the UL-94 test.[8,9] Incorporating 20 wt % APP significantly increases the LOI up to 30.5%, whereas the presence of 5 wt % CNF hardly affects the LOI value of the PLA. By contrast, the LOI values of PLA/APP@CNF gradually increase with increase in the loading level of APP@CNF. PLA/ 20 wt % APP@CNF shows a high LOI value of 32.5%, an increase by 66.7% in comparison with pristine PLA. In addition, PLA has no rating during UL-94 testing and exhibits no flame retardancy classification. Twenty weight percentage APP makes the PLA pass a UL-94 V-0 level, whereas adding 5 wt % CNF enables PLA to achieve a V-2 rating, indicating limited improvement in the flame retardancy of PLA/5% CNF. In comparison, similar to the LOI change, the addition of APP@ CNF into the PLA matrix leads to remarkably reduced
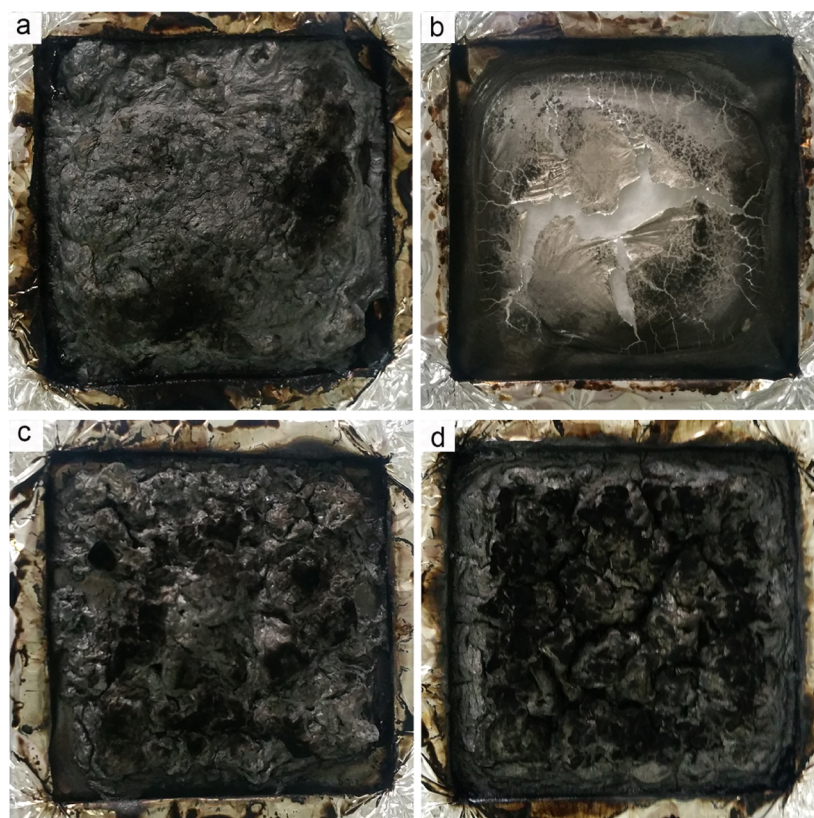
Figure 5. Digital photos for (a) PLA/20APP, (b) PLA/5CNF, (c) PLA/10APP@CNF, and (d) PLA/20APP@CNF.

flammability. Unexpectedly, an APP@CNF loading level as low as 5 wt % can make PLA pass a V-0 rating, implying a high flame-retardant efficiency of APP@CNF in PLA. Comparably, 20 wt % phosphorylated microcrystalline cellulose is still required to enable PLA to achieve a V-0 rating.[25]

The cone calorimeter has been widely used for investigating the fire behavior of polymeric materials to date because it can simulate the real burning behavior of a material.[26−28] Some crucial parameters including heat release rate (HRR), total heat release (THR), and time to ignition (t_{ign}) are exported to quantitatively evaluate the combustion behavior. Figure 4a shows the HRR curves of PLA and its composites, and Table 1 lists the related data. The pure PLA burns vigorously once being ignited, with a peak heat release rate (pHRR) of 434 kW/m^2, and finally generates a THR of 70.1 MJ/m^2. By contrast, although the pHRR and THR of PLA/5CNF are slightly decreased, the dripping obviously disappears due to the suppression action of the high length/diameter ratio of CNF on the melt flow of the PLA during the cone tests. As compared with the PLA matrix, adding 20 wt % APP slightly reduce the t_{ign} to 61 s, the pHRR by 24% (to 328 kW/m^2) and the THR by 33% (47 kW/m^2), indicating significant flame retardancy. By contrast, the addition of 5 wt % CNF shows a t_{ign} of 48 s and a pHRR of 375 kW/m^2, indicating a marginal reduction in flammability. For the PLA/APP@CNF systems, it is clearly indicated that both pHRR and THR parameters effective decrease to different degrees with increasing content of APP@CNF. For PLA/10APP@CNF, pHRR and THR are reduced by 41% (about 255 kW/m^2) and 17% (about 57.9 MJ/m^2) despite a short t_{ign} of 51 s as compared to PLA. Interestingly, after adding 20% APP@CNF, t_{ign} of PLA rebounds up to 60s and the pHRR further reduces to 193 kW/m^2 (a decrease by 56%)

in addition to a THR of 53.6 MJ/m^2. It is worth pointing out that PLA/20APP@CNF shows much lower pHRR values than PLA/5CNF and PLA/20APP, strongly suggesting the synergistic flame retardancy between CNF and APP due to the unique material design and improved fine dispersion.

In addition, the average mass loss rate (AMLR) of PLA composites shows a similar trend to the pHRR. As shown in Figure 4b and Table 1, adding 5% CNF increases, instead of reducing, the AMLR of PLA from 0.079 to 0.1 g/s, implying that the presence of CNF makes the PLA burn faster, whereas the addition of 20% APP can significantly reduce the AMLR down to 0.059 g/s, showing that APP can slow down the combustion process. In comparison, the AMLR seems to monotonously decrease with increasing loading level of APP@CNF in the PLA; for instance, 0.074 g/s for PLA/5APP@CNF, 0.067 g/s for PLA/10APP@CNF, and 0.052 g/s for PLA/20APP@CNF. The steady reduction in AMLR indicates that the presence of APP@CNF can slow down the combustion of PLA. Moreover, the char residues after burning also show a monotonous increase with the increase in APP@CNF content. The char residue of PLA/20APP@CNF composite reaches 14.4 wt %, which is increased by about 96% compared to that of PLA/5CNF composite. In addition, the total smoke production (TSP) of the PLA composites also is given in Table 1. The similar trend to the char residue of PLA composite indicates that the additive APP@CNF suppresses the combustion of the PLA but causes the incomplete burning of volatile matter, thus increasing the TSP of PLA composites. As shown in Table 1, the TSP value of PLA/10APP@CNF and PLA/20APP@CNF is 106.6 and 142.7 m^2/m^2, which is much higher than that of PLA/20APP composite. Combination of all the results of cone,
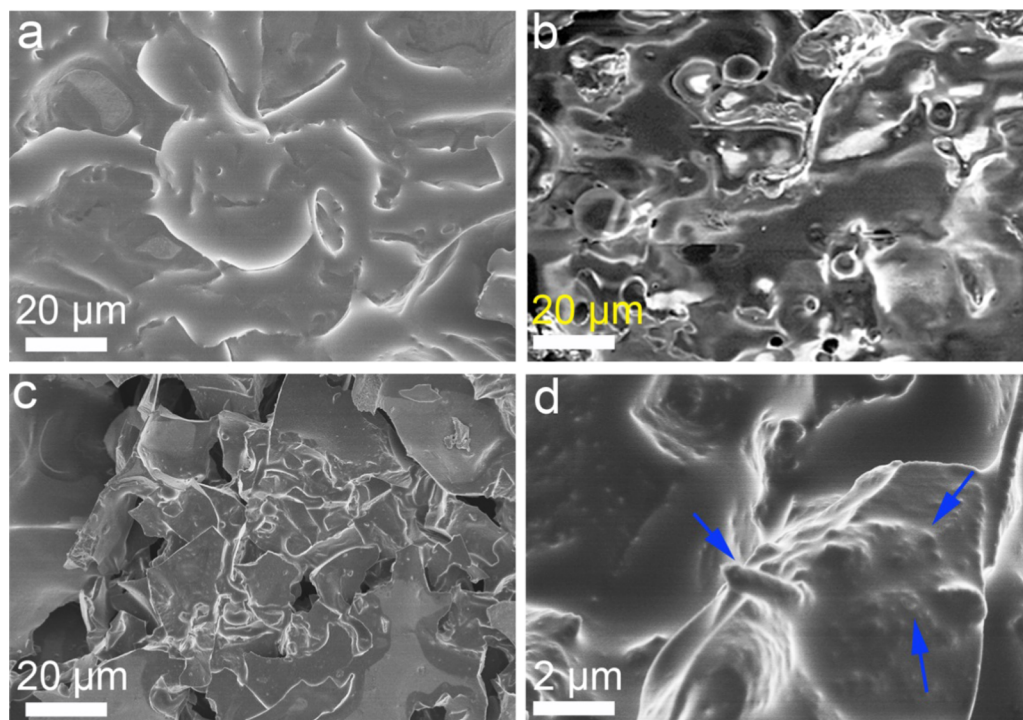
Figure 6. Morphology and chemical structure of residue char for (a) PLA/20APP, (b) PLA/5CNF, and (c, d) PLA/10APP@CNF.
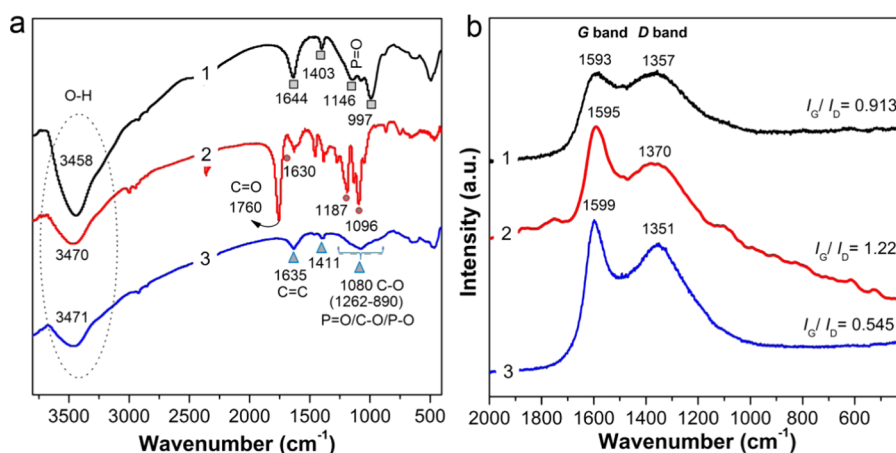
Figure 7. (a) IR spectra and (b) Raman pattern of the residue char for (1) PLA/20APP, (2) PLA/5CNF, and (3) PLA/10APP@CNF systems after cone tests.

LOI, and UL-94 tests strongly indicates that as-designed APP@CNF is a highly efficient flame retardant for PLA.

2.5. Analysis of the Char Residue. To understand how APP@CNF works in terms of reducing the flammability of the PLA, the micromorphology, structure, and chemical composition of the char residues after cone tests are comprehensively examined. Digital photos of the char residues for PLA/20APP, PLA/5CNF, PLA/10APP@CNF, and PLA/20APP@CNF after cone test are shown in Figure 5. In the case of PLA/20APP composite, the residue shows an obvious compact char layer structure despite some cracks (Figure 5a). As for PLA/5CNF, a very thin and fragmented char residue layer after burning can be found in Figure 5b. With regard to PLA/10APP@CNF and PLA/20APP@CNF, the morphologies of the char residues differ substantially from those of PLA/20APP and PLA/5CNF, as shown in Figure 5c,d. The char residues are dense with a few holes, maybe formed by the APP@CNF system. When the content of APP@CNF increases to 20 wt %, the surface morphology of the char residue shows more grid holes but a little collapse, indicating more APP@CNF may cause the char layer to become rigid.

The microstructure of the char residues of the PLA composites is further observed by SEM. As shown in Figure 6a, the char residue of the PLA/APP shows a basically smooth char layer, in good agreement with the relatively good flame retardancy. In the case of the PLA/5CNF (Figure 6b), its char residue exhibits a discontinuous structure with many voids or pores on the surface because of blistering during combustion. Comparably, the char residue of the PLA/10APP@CNF appears as a fibrous network, and the char layer is also intact after fire tests (see Figure 6c). The fibrous char structure may partially inherit from the CNF, as can be clearly observed with the help of a higher magnification (Figure 6d). This chemical fibrous structure also enhances the structural integrity of the
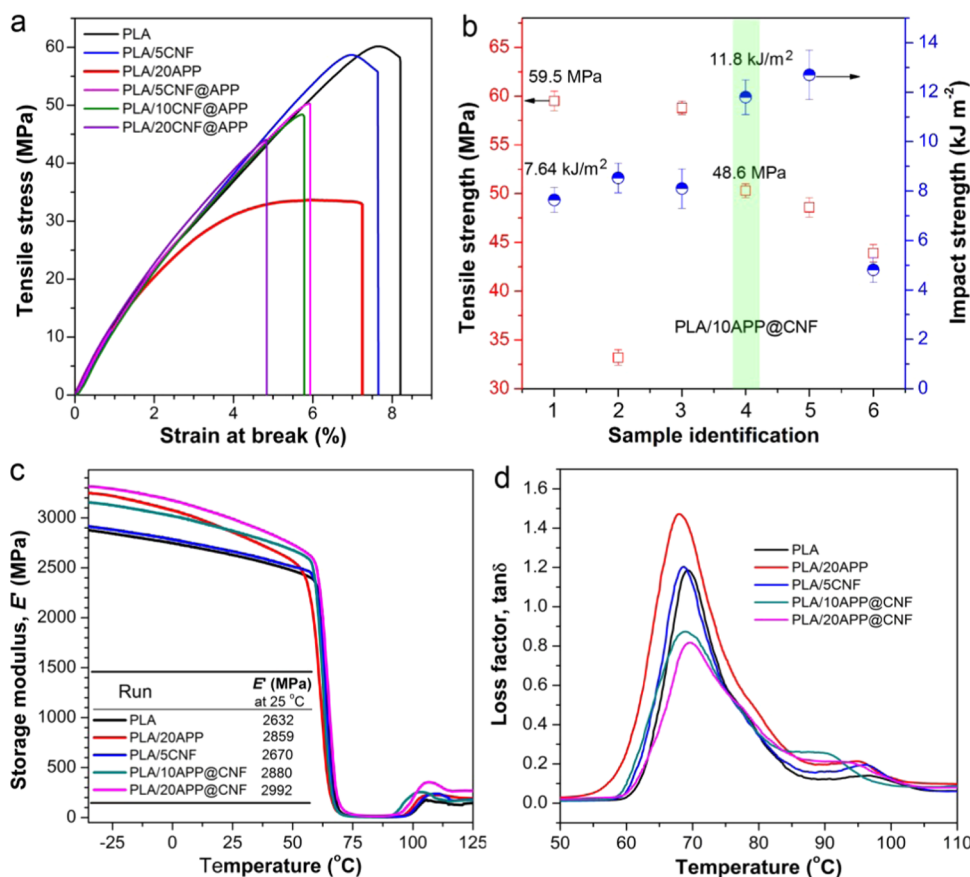
Figure 8. (a) Typical stress−strain curves and (b) tensile strength and impact strength ((1) PLA, (2) PLA/20APP, (3) PLA/5CNF, (4) PLA/5APP@CNF, (5) PLA/10APP@CNF, and (6) PLA/20APP@CNF), (c) storage modulus, and (d) loss factor of PLA and its blends based on APP, CNF, and APP@CNF.

char layer and improves the mechanical strength of the char layer, as marked by blue arrows.

The chemical structure and composition of the char residues of PLA/20APP, PLA/5CNF, and PLA/10APP@CNF were further investigated using FT-IR and Raman spectra. As shown in Figure 7a, the IR spectrum of the char residue of PLA/5CNF typically displays several absorption peaks located at around 3470 cm^{-1} (ν_{O-H}), 1760 cm^{-1} ($\nu_{C=O}$), 1630 cm^{-1} ($\nu_{C=C}$), 1187 cm^{-1} (ν_{C-O}), and 1096 cm^{-1} (ν_{C-OH}). The stretching vibration peak of methylene (CH$_2$) groups is also determined at 2922 cm^{-1}. The spectra of PLA/20APP and PLA/10APP@CNF seem significantly different from those of PLA/5CNF. Specifically, the absorption bands at 1146, 1080, and 997 cm^{-1} are also determined, respectively, belonging to the stretching vibration of P=O, P−O−C, P−O−P groups.[29−31] The existence of these absorption peaks indicates that char layer contains the pyrophosphate species that can catalyze the formation of char residues. Besides, Raman spectroscopy is also used to further characterize the graphitization degree of the char residue. The Raman spectra of the char residue of PLA/5CNF, PLA/20APP, and PLA/10APP@CNF in Figure 7b exhibit two main bands, respectively, located at approximately 1590 cm^{-1} (G band) and 1370 cm^{-1} (D band). G-band corresponds to the vibration of sp^2-hybrided carbon atoms in graphite layers, whereas the D-band represents the sp^3-hybridized carbon and the presence of defect-like amorphous domains.[32,33] From Figure 7b, the G-band and D-band of PLA/5CNF are located at 1595 and 1370 cm^{-1}, demonstrating that graphic and disorder carbon structures are left in the char

residue of PLA/CNF. With respect to PLA/20APP, both G-band and D-band shift to lower wavenumbers, centering at 1593 and 1357 cm^{-1}, respectively, suggesting the catalytic char-forming effect of APP. Compared with PLA/5CNF and PLA/20APP, the char residue of PLA/10APP@CNF shows an increase in G-band (1599 cm^{-1}) and a decrease in D-band (1351 cm^{-1}), primarily due to the catalytic char-forming effect of APP and the participation of CNF in the char-forming process.[34]

Furthermore, the intensity ratio (R) of D-band to G-band (I_D/I_G) can indicate the graphitization degree of the char residue.[33] Generally, a high R value implies a low graphitization degree. The char of PLA/5CNF shows a high I_D/I_G of 1.22, indicating a low graphitization degree. The addition of APP leads the char to show a R value of 0.913, demonstrating a higher graphitization degree. Different from the former two systems, the presence of APP@CNF dramatically decreases the R value to 0.545, indicating that APP@CNF can promote the graphitic order of char.[35]

Based on the above comprehensive analysis of char residues, a possible flame retardancy mechanism of APP@CNF can be proposed. The hybridization via ball-milling in their aqueous solution enables APP@CNF to uniformly disperse within the PLA matrix with smaller phase sizes than APP. Its presence can significantly increase the melt viscosity,[17] reduce HRR, and suppress the combustion behavior of PLA, thereby significantly improving the flame retardancy of PLA. When ignited, the APP in the hybridized flame retardant thermally degrades to create polyphosphate species before the degradation of PLA and CNF

Table 2. Detailed Mechanical Data, Glass Transition Temperature (T_g), and Interfacial Adhesion Parameter of CNF-Based PLA Nanocomposites Obtained by Tensile, Impact, and Dynamic Mechanical Analysis (DMA) Measurements

run	$\sigma_t{}^a$ (MPa)	E^a (GPa)	ε^a (%)	$\sigma_i{}^a$ (kJ/m²)	T_g (°C)	β
PLA	59.5 ± 1.0	2.50 ± 0.05	8.0 ± 0.8	7.64 ± 0.5	69.3	
PLA/20APP	33.2 ± 0.5	2.70 ± 0.07	7.2 ± 0.5	8.53 ± 0.6	67.5	−1.63
PLA/5CNF	58.8 ± 0.7	2.55 ± 0.07	7.5 ± 0.7	8.10 ± 0.8	68.6	−0.195
PLA/5APP@CNF	50.3 ± 0.6	2.69 ± 0.05	5.9 ± 0.6	11.8 ± 0.7		
PLA/10APP@CNF	48.6 ± 1.0	2.73 ± 0.08	5.7 ± 0.7	12.7 ± 1.0	68.9	3.73
PLA/20APP@CNF	43.9 ± 0.9	2.83 ± 0.09	4.9 ± 0.6	4.81 ± 0.5	69.5	2.12

$^a\sigma_t$, E, ε, σ_i, T_g, and β, respectively, represent the tensile strength, Young modulus, stain at break, impact strength, glass transition temperature, and interfacial adhesion parameter.

due to relatively lower thermal stability. Besides the formation of a melt char substance themselves, these polyphosphate species can to some extent catalyze both PLA and CNF to form a continuous, compact layer by dehydration. Meanwhile, the CNF skeleton left in the char during burning can maintain the intact structure of char residue and prevent the char layer from cracking by reinforcing the char. Therefore, APP@CNF strikingly reduces the flammability of PLA by their synergistic work during combustion.

2.6. Mechanical Performances. The mechanical properties of PLA composites are evaluated to verify whether our design can reverse the mechanical compromise. As shown in Figure 8a and Table 2, the pure PLA shows a high tensile strength (σ_t) of about 58.0 MPa, an elastic modulus (E) of about 2.5 GPa, and a strain at break (ε) of only 8.0%. This clearly indicates that the PLA is mechanically brittle. After adding 5.0 wt % CNF, σ_t and E slightly increase. This negligible mechanical change is mainly attributed to the poor dispersion of CNF in the PLA matrix and their weak interfacial adhesion, as evidenced in Figure 2.

With respect to the PLA/20APP system, the presence of APP markedly decreases the tensile strength in spite of a marginally increase in the modulus also because of their poor interfacial compatibility. Theoretically, uniform dispersion, finer phase size, and robust interfacial adhesion can promote efficient transfer of external loads from the polymer matrix to the high-strength CNF.[17,36−39] In addition, the high-strength CNF may also act as a mechanical reinforcing agent for a flame-retardant system. As expected, the presence of 5.0 wt % APP@CNF makes the PLA maintain a high σ_t of 50.3 MPa, despite a slight decrease in E and ε. When 10 wt % APP@CNF is added into the PLA matrix, a high σ_t of 48.6 MPa is still obtained. Further increasing the content of APP@CNF only leads to an improved E and a slightly low σ_t, possibly due to the agglomeration of APP@CNF at a high loading level. However, this strength is still much higher than 33.2 MPa of PLA/20APP, probably because of the improved dispersion and smaller phase sizes, as well as the mechanical reinforcement of CNF on PLA.

Impact strength of PLA and its composites are also measured to evaluate their fracture toughness. As given in Figure 8b and Table 2, the pure PLA shows a low impact strength (σ_i) value of 7.64 kJ/m². As expected, the addition of 5 wt % CNF or 20 wt % APP only shows a marginal impact on σ_i due to poor dispersion and interfaces. In comparison, the addition of 5 wt % APP@CNF improves σ_i to ~11.8 kJ/m², a 54% increase as compared with the PLA matrix, whereas the same addition of CNF only brings a slight improvement, about 8.10 kJ/m². When the loading level reaches 10 wt %, σ_i of PLA increases by 67% (about 12.7 kJ/m²) relative to the PLA bulk. Nevertheless, with the loading of APP@CNF increasing to 20 wt %, σ_i of the

PLA composites sharply decreases to ~4.81 kJ/m², even lower than that of PLA/20APP (~8.53 kJ/m²). This implies that a relatively low loading level of APP@CNF can contribute to the absorption of the impact energy, whereas adding a higher loading over 10 wt % of APP@CNF tends to form stress-concentration sites and leads to reduced fracture toughness because of the formation of agglomeration within the PLA matrix.

Dynamic mechanical analysis (DMA) measurements were also carried out to examine the dynamic mechanical performances of PLA and its biocomposites. The plots of storage modulus (E') and loss factor ($\tan \delta$) curves versus temperature are presented in Figure 8c,d. As also recorded in Table 2, basically the storage modulus displays a similar trend to the elastic modulus obtained by tensile measurements, and the modulus steadily increases with increasing loading level of APP@CNF. The glass transition temperature (T_g) can reflect the interfacial interactions between the filler and the polymer matrix because its value strongly depends on the movement capability of polymer segments. The presence of APP decreases T_g from 69.3 for the PLA matrix to 67.5 °C, indicating the plasticization effect of APP, whereas the CNF hardly affects the T_g value. In comparison, adding 10 and 20% basically makes the PLA maintain its T_g value, which indicates the good interfacial compatibility, although the interface is not strong enough to restrict the movement of PLA chains.

In addition, the peak values of $\tan \delta$ can provide useful information on the interfacial adhesion between the fillers and the PLA matrix, as shown in 1.

$$\frac{(\tan \delta_{max})_c}{(\tan \delta_{max})_m} = 1 - \beta\phi \tag{1}$$

where $(\tan \delta_{max})_c$ and $(\tan \delta_{max})_m$ represent the peak value of $\tan \delta$ of the composites and the polymer matrix obtained by the DMA tests, respectively, ϕ is the volume fraction of the filler, and β refers to the interfacial adhesion parameter. Generally, the larger the β value, the stronger the interfacial adhesion.[40] As shown in Table 2, both PLA/CNF and PLA/APP systems show negative β values (−0.195 and −1.63, respectively), strongly indicating their poor interfacial adhesion and even thermodynamic exclusivity with the PLA matrix due to their big polarity difference. By contrast, β values of 3.73 and 2.12 are obtained for PLA/10APP@CNF and PLA/20APP@CNF, respectively. The big β values are correlated with the stronger interfacial adhesion. The smaller β value for the latter is due to the possible agglomeration of the higher content of APP@ CNF, as evidenced by their tensile strength and impact strength comparisons.

To understand the mechanical failure mechanism, the fracture morphology of the cross section of the PLA
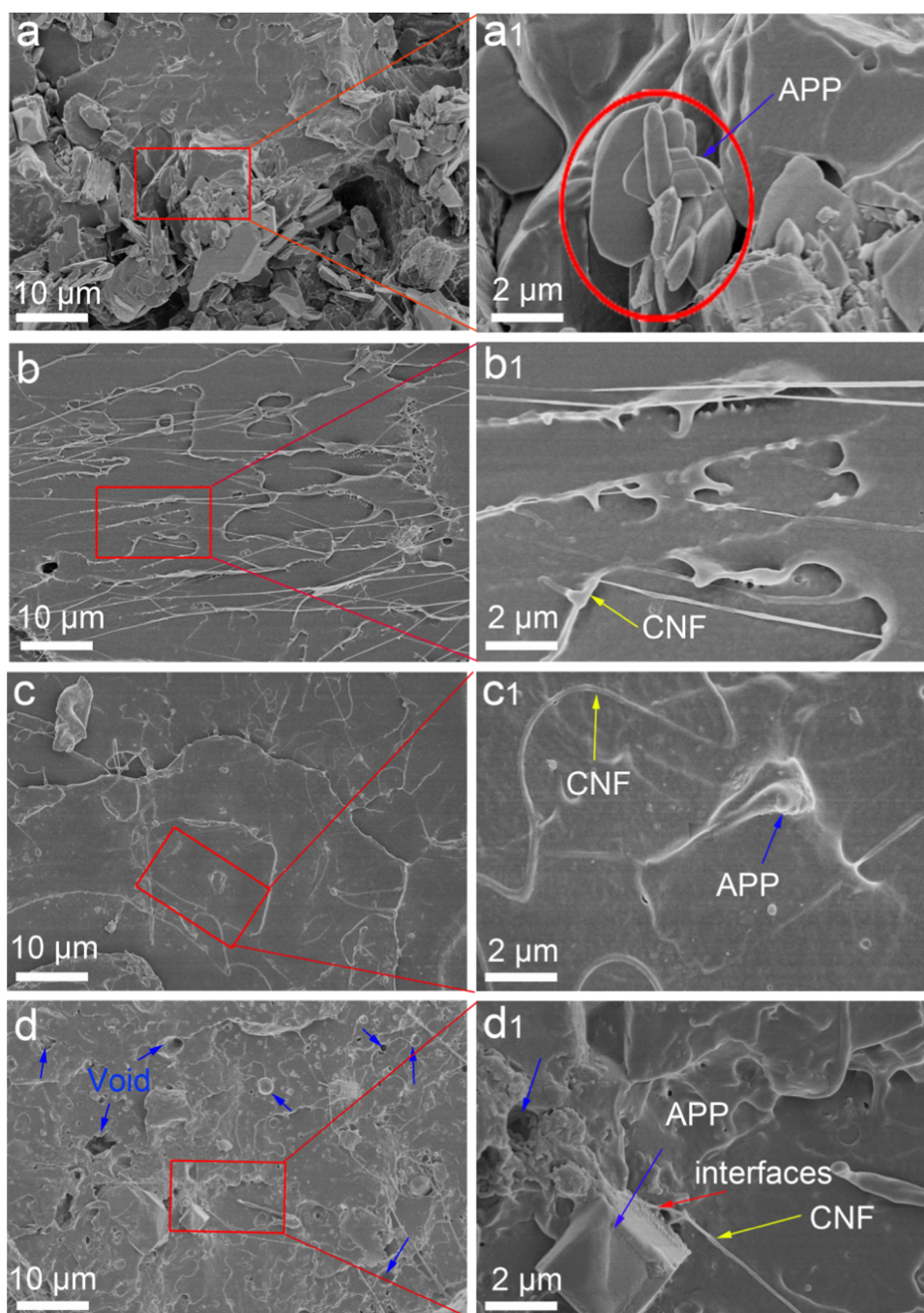
Figure 9. SEM images of fracture surface of (a, a1) PLA/20APP, (b, b1) PLA/5CNF, (c, c1) PLA/10APP@CNF, and (d, d1) PLA/20APP@CNF after impact failure tests.

biocomposites after impact tests is observed by SEM, as shown in Figure 8. Apparently, the fracture surface of PLA/20APP is rather rough and discontinuous, with many holes and fragments, and many exposed APP found at a higher magnification (see Figure 9a,a1) indicate poor interfacial adhesion. As for PLA/5CNF in Figure 9b, the addition of CNF facilitates the formation of a relatively integrated fracture surface due to relatively improved interfacial interactions between the CNF and the PLA matrix, as also evidenced by their close tensile strength values. As seen in Figure 9b1, with higher magnification, some individual CNF can be found to be coated by the polymer layer, further revealing the strong interface. By contrast, a much more continuous, smooth, and

uniform surface morphology of the fracture surface of PLA/10APP@CNF is exhibited in Figure 9c,c1, indicating a good interfacial compatibility between APP@CNF and the PLA matrix and a relatively fine dispersion. This is in good accordance with the above mechanical results. However, the fracture surface of PLA/20APP@CNF becomes nonhomogeneous and shows a porous structure with many voids, some APP agglomerates, and fracture interfaces (Figure 9d,d1), despite strong interfacial interactions among the three components. This can also explain why PLA/20APP@CNF shows a smaller β value than PLA/10APP@CNF. In brief, APP@CNF can form a relatively strong interfacial adhesion with the PLA matrix, thus leading to the high mechanical

strength than APP because CNF can serve as the surface modifier for APP during ball-milling and interfacial compatibilizer between PLA and APP in the composites.

3. CONCLUSIONS

In this work, we have successfully designed a new type of green hybridized flame-retardant system (APP@CNF) by twining APP with CNF as the surface modifier during ball-milling process based on their strong H-bond interactions. APP@CNF can be uniformly dispersed into the PLA matrix in the form of small phase sizes. The addition of only 5.0 wt % APP@CNF enables PLA to achieve a UL-94 V-0 rating in addition to a LOI of 27.5%. The enhanced flame retardancy of APP@CNF in PLA is primarily due to the catalytic char-forming capability of APP and the synergistic effect of CNF by reinforcing the char layer. Incorporating 5.0 wt % of APP@CNF allows the flame-retardant PLA composite to maintain a high tensile strength of 50.3 MPa. Moreover, as compared to the PLA matrix, the impact strength is increased by 54%, reaching 11.8 kJ/m², which is much higher than that of the PLA/APP and PLA/CNF systems. This work offers a facile green strategy to create high-performance, ecofriendly flame retardants and their advanced polymer composites. It can also contribute to expanding the potential application of biodegradable PLA in the automobile, packaging, and electric and electronic fields.

4. EXPERIMENTAL SECTION

4.1. Materials. Poly(lactic acid) (PLA, 4032D) was obtained from Natureworks LLC. Ammonium polyphosphate (APP, CK-APP101, $n > 1000$) was provided by Puyang Chengke Chemical Technology Co., Ltd. (Henan, China). Cellulose nanofiber (CNF, KY100) solid with 25 wt % CNF and 75 wt % water was purchased from Daicel Chemical Industries Co., Ltd. (Japan). Other chemical agents were purchased from Sinopharm Chemical Reagent Co. Ltd. (Shanghai, China). All the chemical reagents were of analytical grade and used without further purification.

4.2. Preparation of APP@CNF. One gram of CNF was added into 99 mL deionized water with the aid of high-speed dispersion (T81 IKA, Germany) to prepare a 1.0 wt% CNF mixture. Then, a certain amount of APP was put into the above suspension under magnetic stirring, and the mass ratio of APP/CNF was 6/1. Subsequently, the mixture was placed into an agate ball-mill capsule (250 mL) containing agate balls (diameter ranging from 1 to 5 mm). The capsule was fixed in the planetary ball-mill machine and agitated at 400 rpm for 8 h. Finally, the resultant product was obtained by filtrating and drying at 80 °C under reduced pressure until the weight did not change. A white solid powder was obtained and designated as APP@CNF, and its typical synthetic route is shown in Figure 1a.

4.3. Composites Fabrication. The PLA composites were prepared by melt compounding of PLA, APP, CNF, or APP@CNF using a ThermoHaake Torque Rheometer with a rotor speed of 60 rpm at 170 °C for 10 min. The formulations of the samples are designed as follows: PLA/xAPP, PLA/xCNF, and PLA/xAPP@CNF, x refers to the mass fraction of APP@CNF in the composite; for example, PLA/20APP containing 20 wt % APP and 80 wt % PLA. Other composites were also prepared according to the same protocol for comparison, respectively.

4.4. Characterization. The FT-IR spectra were recorded on a Bruker Vector 22 FT-IR spectrometer. The sample powders were mixed with KBr. Transmission electron microscopy (TEM; JEM-1200EX) was employed to observe the morphologies of CNF, APP, and APP@CNF, as well as their dispersion in the PLA matrix at 200 kV. The microstructure of the PLA composites was investigated by scanning electron microscopy (SEM, FEI-SEM, Japan), with an accelerating voltage of 15 kV. Thermogrametric analysis (TGA) was carried out on a TA SDTQ600 (TA Instruments) thermogravimetric analyzer at a heating rate of 20 °C/min under N₂ or air atmosphere. The Raman spectra of char were obtained on a Nicolet Almega dispersive Raman spectrometer (Thermo Scientific) with a 514 nm laser source. The Fire behavior of the samples was evaluated by a free time test U.K. device according to ISO 5660 with an incident flux of 35 kW/m². The samples with a size of 100 × 100 × 3.0 mm³ were wrapped in an aluminum foil. Limited oxygen index values (LOI) were measured using an HC-2 oxygen index instrument on 120 × 6 × 3 mm³ sheets according to the standard oxygen index test ASTM D2863. The UL-94 vertical burning tests were conducted by Jiangning CZF-3 vertical burning test instrument according to ASTM D3801 standard. The dimensions of samples were 130 × 13 × 3 mm³. The tensile and impact properties of the samples were measured on a WD-5 electronic universal tensile tester and a Charpy impact tester, according to ASTM 638-03 and GB/T 1043-93, respectively. Dynamic mechanical analyzer (DMA242C, TA) was used to conducted the dynamic mechanical analysis (DMA) of the PLA composites from −40 to +130 °C at a frequency of 1 Hz with a heating rate of 3 °C/min. The glass transition temperature (T_g) was determined from the peak of loss factor (tan δ) versus temperature plots.

The phase sizes of APP and APP@CNF within the PLA matrix were analyzed by image analysis software via micrographs, and over 100 particles were chosen. The weight-average diameter (d_w) of the particles was calculated according to the following 2

$$d_w = \frac{\sum n_i d_i^2}{\sum n_i d_i} \tag{2}$$

Weight-average particle size (d_w), where n_i is the number of particles with a size of d_i.

■ AUTHOR INFORMATION

Corresponding Authors
*E-mail: pingansong@gmail.com (P.S.).
*E-mail: Jinfengdai0601@gmail.com (J.D.).
*E-mail: menglinh@hit.edu.cn (L.M.).

ORCID ⓘ
Pingan Song: 0000-0003-1082-652X

Notes
The authors declare no competing financial interest.

■ REFERENCES

(1) Costes, L.; Laoutid, F.; Brohez, S.; Dubois, P. Bio-based flame retardants: When nature meets fire protection. *Mater. Sci. Eng., R* **2017**, *117*, 1−25.

(2) Bourbigot, S.; Fontaine, G. Flame retardancy of polylactide: an overview. *Polym. Chem.* **2010**, *1*, 1413−1422.

(3) Zhao, C. X.; Liu, Y.; Wang, D. Y.; Wang, D. L.; Wang, Y. Z. Synergistic effect of ammonium polyphosphate and layered double hydroxide on flame retardant properties of poly(vinyl alcohol). *Polym. Degrad. Stab.* **2008**, *93*, 1323−1331.

(4) Li, B.; Dong, F. X.; Wang, X. L.; Yang, J.; Wang, D. Y.; Wang, Y. Z. Organically modified rectorite toughened poly(lactic acid): nanostructures, crystallization and mechanical properties. *Eur. Polym. J.* **2009**, *45*, 2996−3003.

(5) Karamanlioglu, M.; Preziosi, R.; Robson, G. D. Abiotic and biotic environmental degradation of the bioplastic polymer poly(lactic acid): a review. *Polym. Degrad. Stab.* **2017**, *137*, 122−130.

(6) Kimura, K.; Horikoshi, Y. Bio-based polymers. *Fujitsu Sci. Tech. J.* **2005**, *41*, 173−180.

(7) Bourbigot, S.; Fontaine, G. Flame retardancy of polylactide: an overview. *Polym. Chem.* **2010**, *1*, 1413−1422.

(8) Song, Y. P.; Wang, D. Y.; Wang, X. L.; Lin, L.; Wang, Y. Z. A method for simultaneously improving the flame retardancy and toughness of PLA. *Polym. Adv. Technol.* **2011**, *22*, 2295−2301.

(9) Wang, D. Y.; Song, Y. P.; Lin, L.; Wang, X. L.; Wang, Y. Z. A novel phosphorus-containing poly(lactic acid) toward its flame retardation. *Polymer* **2011**, *52*, 233−238.

(10) Cao, Z. H.; Zhang, Y.; Song, P. A.; Cai, Y. Z.; Guo, Q.; Fang, Z. P.; Mao, P. A novel zinc chelate complex containing both phosphorus and nitrogen for improving the flame retardancy of low density polyethylene. *J. Anal. Appl. Pyrolysis* **2011**, *92*, 339−346.

(11) Wei, L. L.; Wang, D. Y.; Chen, H. B.; Chen, L.; Wang, X. L.; Wang, Y. Z. Effect of phosphorus-containing flame retardant on the thermal and early flaming behaviors of poly(lactic acid). *Polym. Degrad. Stab.* **2011**, *96*, 1557−1561.

(12) Yuan, X. Y.; Wang, D. Y.; Chen, L.; Wang, X. L.; Wang, Y. Z. Inherent flame retardation of bio-based poly(lactic acid) by incorporating phosphorus linked pendent group into the backbone. *Polym. Degrad. Stab.* **2011**, *96*, 1669−1675.

(13) Mauldin, T. C.; Zammarano, M.; Gilman, J. W.; Shields, J. R.; Boday, D. J. Synthesis and characterization of isosorbide-based polyphosphonates as biobased flame-retardants. *Polym. Chem.* **2014**, *5*, 5139−5146.

(14) Zhao, X. M.; Guerrero, F. R.; Llorca, J.; Wang, D. Y. New supereffciently flame-retardant Bioplastic poly(lactic acid): flammability, thermal decomposition behavior, and tensile properties. *ACS Sustainable Chem. Eng.* **2016**, *4*, 202−209.

(15) Yu, T.; Jiang, N.; Li, Y. Functionalized multi-walled carbon nanotube for improving the flame retardancy of ramie/poly(lactic acid) composite. *Compos. Sci. Technol.* **2014**, *104*, 26−33.

(16) Qian, Y.; Wei, P.; Jiang, P. K.; Li, Z.; Yan, Y. G.; Ji, K. J. Aluminated mesoporous silica as novel high-effective flame retardant in polylactide. *Compos. Sci. Technol.* **2013**, *82*, 1−7.

(17) Feng, J.; Sun, Y.; Song, P. A.; Lei, W.; Wu, Q.; et al. Fire-Resistant, Strong, and Green Polymer Nanocomposites Based on Poly(lactic acid) and Core-Shell Nanofibrous Flame Retardants. *ACS Sustainable Chem. Eng.* **2017**, *5*, 7894−7904.

(18) Sturcová, A.; Davies, G. R.; Eichhorn, S. J. Elastic modulus and stress-transfer properties of tunicate cellulose whiskers. *Biomacromolecules* **2005**, *6*, 1055−1061.

(19) Klemm, D.; Kramer, F.; Moritz, S.; lindström, T.; Ankerfors, M.; Gray, D.; Dorris, A. Nanocelluloses: a new family of nature-based materials. *Angew. Chem., Int. Ed.* **2011**, *50*, 5438−5466.

(20) Yano, H.; Sugiyama, J.; Nakagaito, A. N.; Nogi, M.; Matsuura, T.; Hikita, M.; Handa, K. Optically transparent composites reinforced with networks of bacterial nanofibers. *Adv. Mater.* **2005**, *17*, 153−155.

(21) Wang, B.; Tang, Q.; Hong, N.; Song, L.; Wang, L.; Shi, Y.; Hu, Y. Effect of cellulose acetate butyrate microencapsulated ammonium polyphosphate on the flame retardancy, mechanical, electrical, and thermal properties of intumescent flame-retardant ethylene-vinyl acetate copolymer/microencapsulated ammonium polyphosphate/polyamide-6 blends. *ACS Appl. Mater. Interfaces* **2011**, *3*, 3754−3761.

(22) Qian, M.; Sun, Y. Q.; Xu, X. D.; Liu, L. N.; Song, P. A.; Yu, Y. M.; Wang, H.; Qian, J. 2D-alumina platelets enhance mechanical and abrasion properties of PA612 via interfacial hydrogen-bond interactions. *Chem. Eng. J.* **2016**, *308*, 760−771.

(23) Song, P.; Xu, Z. G.; Dargusch, M. S.; Chen, Z. G.; Wang, H.; Guo, Q. P. Granular nanostructure: a facile biomimetic strategy for the design of supertough polymeric materials with high ductility and strength. *Adv. Mater.* **2017**, *29*, No. 1704661.

(24) Zhao, X.; Guerrero, F. R.; Llorca, J.; Wang, D. Y. New Superefficiently Flame-Retardant Bioplastic Poly(lactic acid):Flammability, Thermal Decomposition Behavior, and Tensile Properties. *ACS Sustainable Chem. Eng.* **2016**, *4*, 202−209.

(25) Huang, G. B.; Wang, S. Q.; Song, P. A.; Wu, C. L.; Chen, S. Q.; Wang, X. Combination effect of carbon nanotubes with graphene on intumescent flame-retardant polypropylene nanocomposites. *Composites, Part A* **2014**, *59*, 18−25.

(26) Liu, L. N.; Qian, M. B.; Song, P. A.; Huang, G. B.; Yu, Y. M.; Fu, S. Y. Fabrication of green lignin-based flame retardants for enhancing the thermal and fire retardancy properties of polypropylene/wood composites. *ACS Sustainable Chem. Eng.* **2016**, *4*, 2422−2431.

(27) Song, P. A.; Wang, C.; Chen, L.; Zheng, Y. Q.; Liu, L. N.; Wu, Q.; Huang, G. B.; Yu, Y. M.; Wang, H. Thermally stable, conductive and flame-retardant nylon 612 composites created by adding two-dimensional alumina platelets. *Composites, Part A* **2017**, *97*, 100−110.

(28) Yu, Y.; Fu, S.; Song, P. A.; Luo, X.; Jin, Y.; Lu, F.; Wu, Q.; Ye, J. Functionalized lignin by grafting phosphorus-nitrogen improves the thermal stability and flame retardancy of polypropylene. *Polym. Degrad. Stab.* **2012**, *97*, 541−546.

(29) Bourbigot, S.; Bras, M. L.; Delobel, R. Carbonization mechanisms resulting from intumescence association with the ammonium polyphosphate-pentaerythritol fire retardant system. *Carbon* **1993**, *31*, 1219−1230.

(30) Yu, Y.; Song, P. A.; Jin, C.; Fu, S.; Zhao, L.; Wu, Q.; Ye, J. Catalytic Effects of Nickel (Cobalt or Zinc) Acetates on Thermal and Flammability Properties of Polypropylene-Modified Lignin Composites. *Ind. Eng. Chem. Res.* **2012**, *51*, 12367−12374.

(31) Bourbigot, S.; Bras, M. L.; Delobel, R.; Bréant, P.; Trémillon, J. M. Carbonization mechanisms resulting from intumescence-part II. Association with an ethylene terpolymer and the ammonium polyphosphate-pentaerythritol fire retardant system. *Carbon* **1995**, *33*, 283−294.

(32) Tao, T.; Chen, X.; Meng, X.; Hui, C.; Ding, Y. Synthesis of multiwalled carbon nanotubes by catalytic combustion of polypropylene. *Angew. Chem., Int. Ed.* **2005**, *44*, 1517−1520.

(33) Tuinstra, F.; Koenig, J. L. Raman Spectrum of Graphite. *J. Chem. Phys.* **1970**, *53*, 1126−1130.

(34) Song, R.; Zhang, B.; Huang, B.; Tang, T. Synergistic effect of supported nickel catalyst with intumescent flame-retardants on flame retardancy and thermal stability of polypropylene. *J. Appl. Polym. Sci.* **2006**, *102*, 5988−5993.

(35) Wang, C. S.; Shieh, J. Y.; Sun, Y. M. Phosphorus containing PET and PEN by direct esterification. *Eur. Polym. J.* **1999**, *35*, 1465−1472.

(36) Zhao, X.; Llorca, J.; Wang, D. Y.; et al. Impact of halogen-free flame retardant with varied phosphorus's chemical surrounding on the properties of diglycidyl ether of bisphenol-A type epoxy resin: Synthesis, Fire behavior, Flame-retardant Mechanism and Mechanical Properties. *RSC Adv.* **2016**, *6*, 59226−59236.

(37) Xu, X.; Liu, F.; Jiang, L.; Zhu, J. Y.; Haagenson, D.; Wiesenborn, D. P. Cellulose nanocrystals vs cellulose nanofibrils: A comparative study on their microstructures and effects as polymer reinforcing agents. *ACS Appl. Mater. Interfaces* **2013**, *5*, 2999−3009.

(38) Song, P. A.; Xu, L. H.; Guo, Z. H.; Zhang, Y.; Fang, Z. P. Flame retardant wrapped carbon nanotubes for simultaneously improving the flame retardancy and mechanical properties of polypropylene. *J. Mater. Chem.* **2008**, *18*, 5083−5091.

(39) Song, P. A.; Xu, Z. G.; Guo, Q. P. Bioinspired strategy to reinforce PVA with improved toughness and thermal properties via hydrogen-bond self-assembly. *ACS Macro Lett.* **2013**, *2*, 1100−1104.

(40) Goriparthi, B. K.; Suman, K. N. S.; Mohan Rao, N. Effect of fiber surface treatments on mechanical and abrasive wear performance of polylactide/jute composites. *Composites, Part A* **2012**, *43*, 1800−1808.